



OPEN

Exact dimer phase with anisotropic interaction for one dimensional magnets

Hong-Ze Xu¹, Shun-Yao Zhang¹, Guang-Can Guo^{1,2,3} & Ming Gong^{1,2,3}✉

We report the exact dimer phase, in which the ground states are described by product of singlet dimer, in the extended XYZ model by generalizing the isotropic Majumdar–Ghosh model to the fully anisotropic region. We demonstrate that this phase can be realized even in models when antiferromagnetic interaction along one of the three directions. This model also supports three different ferromagnetic (FM) phases, denoted as x-FM, y-FM and z-FM, polarized along the three directions. The boundaries between the exact dimer phase and FM phases are infinite-fold degenerate. The breaking of this infinite-fold degeneracy by either translational symmetry breaking or \mathbb{Z}_2 symmetry breaking leads to exact dimer phase and FM phases, respectively. Moreover, the boundaries between the three FM phases are critical with central charge $c = 1$ for free fermions. We characterize the properties of these boundaries using entanglement entropy, excitation gap, and long-range spin-spin correlation functions. These results are relevant to a large number of one dimensional magnets, in which anisotropy is necessary to isolate a single chain out from the bulk material. We discuss the possible experimental signatures in realistic materials with magnetic field along different directions and show that the anisotropy may resolve the disagreement between theory and experiments based on isotropic spin-spin interactions.

The spin models for magnetism are basic topics in modern solid-state physics and condensed matter physics¹. In these models, only a few of them mostly focused on low dimensions, can be solved exactly. In general, we may categorize these solvable models into two different groups according to the methods these models are solved.

In the first group, the models can be solved exactly using some mathematical techniques based on their symmetries² and the dual relation between fermions and spins. Typical examples are the transverse Ising model, the XY model, the XXZ model^{3–5}, the XYZ model^{6–8}, and the toric code model^{9,10}. Here, the XY model and Ising model can be mapped to the non-interacting *p*-wave superconducting model by a non-local Jordan–Wigner transformation, which can then be solved by a unitary transformation in the momentum space^{11–15}. The XXZ model is a prototype model for the exact calculation by the Bethe-ansatz approach. In combination with the Jordan–Wigner transformation, the XXZ model is mapped to the interacting Hubbard model, for which reason some of the Hubbard models may also be solved using the Bethe-ansatz approach by Lieb and Wu¹⁶. The XYZ model can also be solved analytically by the off-diagonal Bethe-ansatz method⁶ and modular transformations method^{7,8}. The Bethe-ansatz approach has broad applications in many-body physics. With the above approaches, their spectra, partition function and correlation functions of these models can be obtained exactly. Recently, the spinon excitations in these models have been directly measured in experiments by neutron diffraction^{17–19}. In the two dimensional models, the Kitaev toric code model can be solved exactly by considering the gauge symmetries in each plateau^{9,10}. These solvable models have also played an essential role in the understanding of the non-equilibrium dynamics, phase transitions, and entanglement in the many-body systems^{15,20–23}.

In the second group, which is most relevant to the research in this work, only the ground states (GSs) of the Hamiltonian can be obtained. For example, in the most representative spin-1/2 Majumdar–Ghosh (MG) model^{24–29}, which reads as

¹CAS Key Laboratory of Quantum Information, University of Science and Technology of China, Hefei 230026, China. ²Synergetic Innovation Center of Quantum Information and Quantum Physics, University of Science and Technology of China, Hefei 230026, Anhui, China. ³CAS Center For Excellence in Quantum Information and Quantum Physics, University of Science and Technology of China, Hefei 230026, Anhui, China. ✉email: gongm@ustc.edu.cn

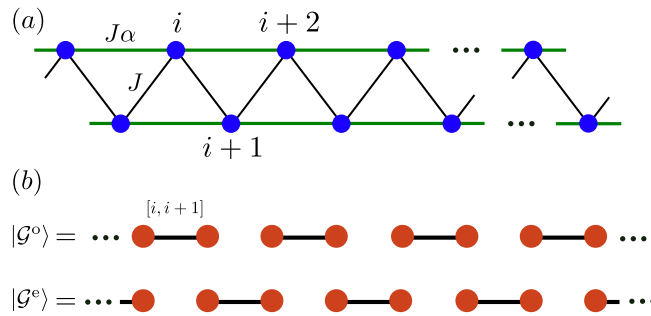


Figure 1. (a) The model in Eq. (9) with nearest J and next-nearest-neighbor interaction $J\alpha$. (b) The schematic illustration of the two exact dimer states, in which each singlet dimer is represented by a solid bound (see the exact definition of the wave function in Eq. (7)).

$$H_{MG} = J \sum_i^L (h_{i,i+1}^0 + \alpha h_{i,i+2}^0), \tag{1}$$

with

$$h_{ij}^0 = s_i^x s_j^x + s_i^y s_j^y + s_i^z s_j^z = \mathbf{s}_i \cdot \mathbf{s}_j, \quad \alpha = \frac{1}{2}. \tag{2}$$

This model can be obtained from the Fermi-Hubbard by second-order exchange interaction, thus $J > 0$ for anti-ferromagnetic interaction. The GSs of the above model can be expressed exactly as the product of singlet dimers. This model preserves the three \mathbb{Z}_2 symmetries by defining $s_i^x \rightarrow -s_i^x, s_i^y \rightarrow -s_i^y$ and $s_i^z \rightarrow s_i^z$ and its index rotation. Using the above Jordan–Wigner transformation, the next-nearest-neighbor interaction and the coupling along the z -direction can yield complicated many-body interaction, thus this model can not be solved analytically using the approach in the first group. However, the GSs can be constructed using some special tricks with the help of the projector operators. Let us define $\mathbf{\Pi} = \mathbf{s}_i + \mathbf{s}_{i+1} + \mathbf{s}_{i+2}$, with $s_i^2 = (s_i^x)^2 + (s_i^y)^2 + (s_i^z)^2 = \frac{3}{4}$, we can obtain

$$\mathbf{\Pi}^2 = \frac{9}{4} + 2(\mathbf{s}_i \cdot \mathbf{s}_{i+1} + \mathbf{s}_i \cdot \mathbf{s}_{i+2} + \mathbf{s}_{i+1} \cdot \mathbf{s}_{i+2}) = S(S + 1), \tag{3}$$

with $S = \frac{1}{2}$ or $\frac{3}{2}$ from the decoupling $\frac{1}{2} \otimes \frac{1}{2} \otimes \frac{1}{2} = \frac{1}{2} \oplus \frac{1}{2} \oplus \frac{3}{2}$. The above result means that the total spin space can be decoupled into three different irreducible representations. Let us define the corresponding projectors for these subspaces as $P_S(i, i + 1, i + 2)$, then we have

$$\mathbf{s}_i \cdot \mathbf{s}_{i+1} + \mathbf{s}_i \cdot \mathbf{s}_{i+2} + \mathbf{s}_{i+1} \cdot \mathbf{s}_{i+2} = \frac{3}{2} P_{\frac{3}{2}}(i, i + 1, i + 2) - \frac{3}{4}. \tag{4}$$

The projectors have the feature that $P_S(i, i + 1, i + 2)P_S(i, i + 1, i + 2) = \delta_{SS}P_S(i, i + 1, i + 2)$ and $\langle \psi | P_S(i, i + 1, i + 2) | \psi \rangle \geq 0$ for any wave function. Then MG model of Eq. (1) can be rewritten as

$$\begin{aligned} H_{MG} &= J \sum_i^L \frac{3}{4} \left[P_{\frac{3}{2}}(i, i + 1, i + 2) - \frac{1}{2} \right] \\ &= -\frac{3}{8} JL + \frac{3J}{4} \sum_i P_{\frac{3}{2}}(i, i + 1, i + 2). \end{aligned} \tag{5}$$

Here the project in the singlet subspace $P_{1/2}$ is absent from the Hamiltonian. The GSs energy of H_{MG} is given by $-\frac{3}{8}L$, which means that for any i , the ground state $|\mathcal{G}\rangle$ should satisfy

$$P_{\frac{3}{2}}(i, i + 1, i + 2)|\mathcal{G}\rangle = 0. \tag{6}$$

This constraint requires $J > 0$; otherwise, the triplet state(s) should have much lower energy. To this condition, there must be a singlet in the three adjacent sites for the eigenvectors of $P_{1/2}(i, i + 1, i + 2)$. Mathematically, the two exact dimer GSs can be written as

$$|\mathcal{G}^e\rangle = \prod_{2n} [2n, 2n + 1], \quad |\mathcal{G}^o\rangle = \prod_{2n} [2n - 1, 2n], \tag{7}$$

where $[i, i + 1] = \frac{1}{\sqrt{2}} | \uparrow_i \downarrow_{i+1} - \downarrow_i \uparrow_{i+1} \rangle$ represents the singlet dimer between neighboring sites (see Fig. 1b with solid bounds). This idea was generalized to the Affleck–Kennedy–Lieb–Tasaki (AKLT) model in a spin-1 chain with

$$H^{\text{AKLT}} = J \sum_i \mathbf{s}_i \cdot \mathbf{s}_{i+1} + \frac{1}{3} (\mathbf{s}_i \cdot \mathbf{s}_{i+1})^2, \quad (8)$$

which was one of the most important models for the Haldane phase^{30–33}. The degeneracy of the GSs of this model can be solved using the above constructive approach. The AKLT model is also one of the basic models for the searching of symmetry protected topological (SPT) phases, which are frequently searched by the above construction method.

The MG model may be relevant to a large number of one dimensional magnets in experiments in solid materials, such as CuGeO_3 ^{34–36}, TiOCl ^{37,38}, $\text{Cu}_3(\text{MoO}_4)(\text{OH})_4$ ³⁹, DF_5PNN ⁴⁰, $(\text{TMTTF})_2\text{PF}_6$ ⁴¹, $(\text{o-Me}_2\text{TTF})_2\text{NO}_3$ ⁴² and $\text{MEM}(\text{TCNQ})_2$ ⁴³, etc. In these materials, the lattice constant along one of the directions is much smaller than the other two directions, rendering the couplings between the magnetic atoms along the shortest lattice constant direction is much stronger than along the other two directions, giving rise to one dimensional magnets. To date, most of these candidates are explained based on the isotropic spin models. It was found that these isotropic models are insufficient to understand all results in experiments^{44–46}.

There are two major starting points for this work. Firstly, we hope to generalize the physics discussed in the isotropic models to the fully anisotropic models, which may contain some beautiful mathematical structures. Secondly, we hope to provide a possible model to study the one dimensional magnets observed in experiments, as above mentioned, which contain some more possible tunable parameters while the fundamental physics is unchanged. In other words, the physics based on isotropic interaction can be found in some more general Hamiltonians. Our model harbors not only the exact dimer phase, but also three gapped ferromagnetic (FM) phases, denoted as x -FM, y -FM and z -FM, according to their magnetic polarization directions. We can determine their phase boundaries analytically based on a simplified model assuming exact dimerization. We find that the boundaries between exact dimer phase and FM phases are infinite-fold degenerate, while the boundaries between the FM phases are gapless and critical with central charge $c = 1$ for free fermions. Thus these two phases represent either the translational symmetry breaking or the \mathbb{Z}_2 symmetry breaking from the infinite-fold degenerate boundaries. We finally discuss the relevance of our results to one dimensional magnets and present evidences to distinguish them in experiments, showing that it explains both the exact dimer phase and the anisotropic susceptibility, which are simultaneously obtained in experiments.

This manuscript is organized as the following. In “[Model and Hamiltonian](#)”, we present our model for the generalized MG model with anisotropic XYZ interaction. In “[Exact dimer phase](#)”, we present a method to obtain the exact dimer phase and the associated phase boundaries. We will map out the whole phase diagram based on this analysis and confirm our results with high accuracy using exact diagonalization method and density matrix renormalization group (DMRG) method. In “[Ferromagnetic phases](#)”, we will discuss the three ferromagnetic phases. In “[Model and Hamiltonian](#)” to “[Ferromagnetic phases](#)”, we mainly discuss the physics in the MG point with $\alpha = 1/2$ for the sake of exact solvability; however, the similar physics will be survived even away from this point. In “[Experimental relevant and measurements](#)”, we will show how this model can find potential applications in some of the one dimensional magnets away from the MG point. Finally, we conclude in “[Conclusion](#)”. Details about the phase boundaries and the general theorem will be presented in the “[Appendix](#)”.

Model and hamiltonian

We consider the following spin-1/2 model directly generalized from the isotropic MG model (see Fig. 1a),

$$H(x, y, z) = J \sum_i^L h_{i,i+1} + \alpha h_{i,i+2}, \quad (9)$$

where $\alpha = \frac{1}{2}$ (MG point) and $J > 0$. For the anisotropic Heisenberg interaction, we have

$$h_{i,j} = xs_i^x s_j^x + ys_i^y s_j^y + zs_i^z s_j^z, \quad (10)$$

with $x, y, z \in \mathbb{R}$. Hereafter, we let $J = 1$, unless specified. The case when $x = y = z > 0$ corresponds to the well-known MG model with exact dimer phase based on isotropic interaction^{24,25}. Anisotropy can be introduced to this model by letting $x = y > 0$, in which when $z > -x/2$ the GSs are also exactly dimerized with XXX interaction^{47–49}.

There are several ways to extend this model to more intriguing and more realistic conditions, considering the possible anisotropy in real materials. For example, in the presence of some proper long-range interactions⁵⁰, the GSs can still be exactly dimerized using the constructive approach in “[Introduction](#)”. When this model is generalized to integer spins, it may support SPT phases^{51–54}. However, in the presence of anisotropy as discussed above, which can not be solved analytically, the physics is largely unclear.

Exact dimer phase

Our phase diagram of the exact dimer phase for Eq. (9) is presented in Fig. 2. This phase has the advantage to be determined exactly with even small lattice sites with periodic boundary condition (PBC). We will confirm the analytical phase boundary with high accuracy using numerical methods.

Phase boundary. The exact dimer states in Eq. (7) are independent of system parameters, indicating that it is also exact even in a finite system. To this end, we consider the simplest case with $L = 4$ with Hamiltonian as

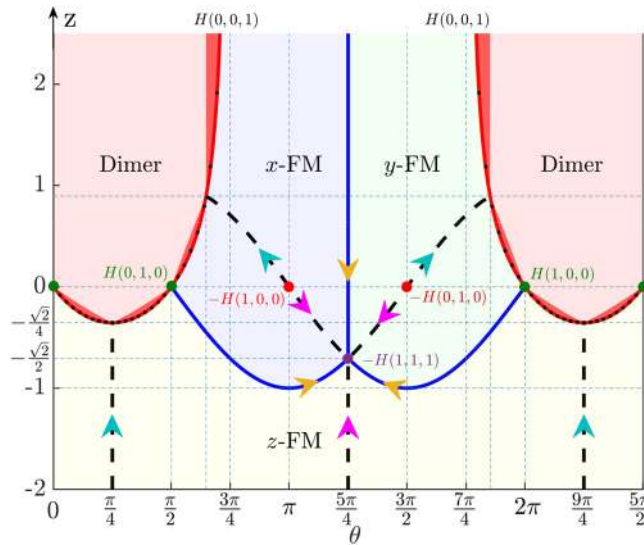


Figure 2. Phase diagram for the fully anisotropic XYZ model in Eq. (9). We have assumed $x = \cos(\theta)$ and $y = \sin(\theta)$. The phase boundaries between exact dimer phase and FM phases are determined by Eq. (13), while the dots are boundaries determined by order parameters, with absolute difference $|z_c - z_{ex}|$ (z_{ex} is the exact boundary given by Eq. (13)) less than 3.0×10^{-4} . In the exact dimer phase, the deep red regions can not be explained by mixing of two anisotropic dimer models; see Eq. (17). The classical limits are denoted as $H(1, 0, 0)$, $H(0, 1, 0)$ and $H(0, 0, 1)$ and the dashed lines are conditions for exact FM states.

$$H_4 = h_{12} + h_{23} + h_{34} + h_{41} + \alpha[h_{13} + h_{24} + h_{31} + h_{42}]. \tag{11}$$

This model can be solved analytically with eigenvalues given below

$$\begin{cases} E_{1-3} = -\frac{x}{2}, & E_{4-6} = -\frac{y}{2}, & E_{7-9} = -\frac{z}{2}, \\ E_{10} = \frac{3x}{2}, & E_{11} = \frac{3y}{2}, & E_{12} = \frac{3z}{2}, \\ E_{13-14} = \frac{1}{2} \left(x + y + z \pm \sqrt{x^2 + y^2 + z^2 - xy - yz - zx} \right), \\ E_{15-16}^{\text{dimer}} = -\frac{x + y + z}{2}. \end{cases} \tag{12}$$

The last two states with two-fold degeneracy correspond to the exact dimer phase with eigenvectors in the form of Eq. (7). One can verify that this model can be solved analytically only at the MG point with $\alpha = 1/2$. To request the exact dimer states have the lowest energy, we request $E_{15-16}^{\text{dimer}} < E_i$ for $i = 1 - 14$, which yields

$$x + y + z > 0, \quad xy + yz + zx > 0. \tag{13}$$

This is the major phase boundary determined for the exact dimer phase (see boundaries in Fig. 2). Let's assume $x + y > 0$, then the second equation yields the exact phase boundary

$$z > z_{ex} = -\frac{xy}{x + y}. \tag{14}$$

The same boundary can be obtained for $L = 6$ and 8 with high accuracy from the eigenvalues and ground state degeneracy (see Fig. 3). By this result, the GSs energy for the exact dimer phase for a chain with length L (L is an even number), following Eq. (12), is given by

$$E_g^{\text{dimer}} = -\frac{(x + y + z)L}{8}. \tag{15}$$

This result naturally includes the previously known results in the MG model with $x = y = z > 0^{50}$ and the extended XXZ model with $x = y > 0$ and $z > -x/2^{47-49}$. The accuracy of this boundary will be checked by the order parameters in the next subsection.

As discussed in the section of the introduction, the ferromagnetic interaction with $J > 0$ is essential for the exact dimer states; otherwise, the triplet state is more energetically favorable (see Eq. (5)). Here, Eq. (13) can lead to an interesting conclusion beyond this criterion that the exact dimer states can be found in the anisotropic model with some kind of antiferromagnetic interaction. For the three parameters in Eq. (9), we find that this exact dimer phase can be realized when only one of the anisotropic parameters is negative valued. It can be

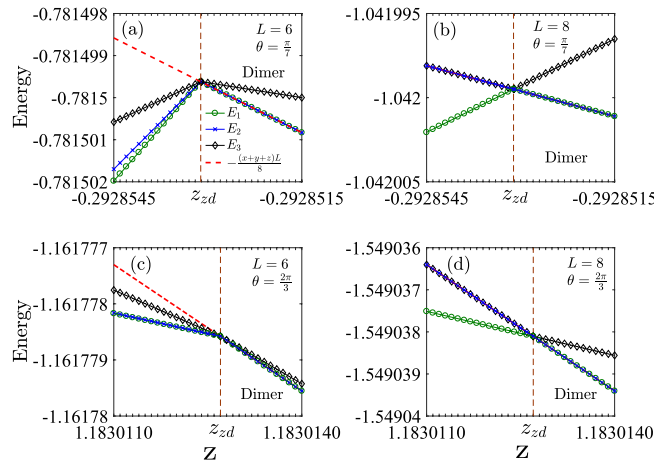


Figure 3. Energy spectra of the lowest three levels for small lattice sites with PBC based on exact diagonalization method. (a, b) show the exact dimer phase boundary ($z_{ex} = -xy/(x + y) = -0.2928531$) at $\theta = \frac{\pi}{7}$ with $L = 6$ and $L = 8$. (c, d) show the exact dimer phase boundary ($z_{ex} = -xy/(x + y) = 1.1830127$) at $\theta = \frac{2\pi}{3}$ with $L = 6$ and $L = 8$. In the exact dimer phase, the GS energy of the two-fold degenerate states is given by Eq. (15) (red dashed lines).

proven as follows. Let y and z be negative values, then $x > |y| + |z| > 0$. However, the second condition in Eq. (13) means $\frac{1}{x} > \frac{1}{|y|} + \frac{1}{|z|}$. The multiply of these two inequalities yields an obvious contradiction. For the case with two negative parameters, one may compute $-H$, which may support exact dimer states in its GSs. In this way, the highest levels of H can be exactly dimerized when Eq. (13) is satisfied.

Then, how to understand the phase boundary in Eq. (13)? Whether this boundary contains some nontrivial region that can not be explained by the known results in the previous literature? To this end, we first need to prove another model for the exact dimer phase. For $z = 0$ and $x > 0, y > 0$, let us define

$$H_{xy} = H(x, y, 0) = \sum_i xh_i^x + yh_i^y, \tag{16}$$

where $h_i^\eta = \frac{1}{2} \sum_i s_i^\eta s_{i+1}^\eta + s_i^\eta s_{i+2}^\eta + s_{i+1}^\eta s_{i+2}^\eta$. We can prove that the minimal energy of h_i^η is $-1/8^{55}$, thus the GSs energy $E_g \geq -(x + y)L/8$, which can be reached by states in Eq. (7). With this model, we may construct a mixed Hamiltonian (see the general theorem for this decoupling in the “Appendix”),

$$H_x = \beta H(x', x', z') + (1 - \beta)H(x'', y'', 0), \tag{17}$$

where $z' > -x'/2, x'' > 0, y'' > 0$ and $\beta \in [0, 1]$. We require that both $H(x', x', z')$ and $H(x'', y'', 0)$ have the same exact dimer GSs of Eq. (7). Then, according to Eq. (13), we can find the exact dimer GSs when

$$\beta(2x' + z') + (1 - \beta)(x'' + y'') > 0, \tag{18}$$

and

$$\beta^2(x'^2 + 2x'z') + (1 - \beta)^2x''y'' + \beta(1 - \beta)(x'' + y'')(x' + z') > 0, \tag{19}$$

which can always be fulfilled for the given condition. So the decoupling of H_x provides a general approach to construct exact dimer GSs from some simple (known) models, which can be used to understand the exact dimer states in some of the regions in the phase diagram of Fig. 2. Nevertheless, not all regions in the phase diagram can be understood in this way. In Eq. (17), one may replace the XXZ model by the anisotropic XYZ model and prove that this decoupling only allows solution when $z > -\frac{1}{2} \min(\cos(\theta), \sin(\theta))$ for $\theta \in [0, \pi/2]$, $z > -2 \cos(\theta)$ for $\theta \in (\pi/2, \pi - \arctan(2))$, and $z > -2 \sin(\theta)$ for $\theta \in (3\pi/2 + \arctan(2), 2\pi)$ (see the light red regions in Fig. 2. The detailed analysis can be found in the “Appendix”. Beyond these three regions, the exact dimer phase can not be understood by the mechanism of Eq. (17), which indicates of non-triviality for this phase.

Order parameters and infinite-fold degeneracy. The boundary condition in Eq. (13) automatically satisfies the permutation symmetry of H . This boundary is numerically verified with extraordinary high accuracy (see the dots in Fig. 2). A typical transition from the exact dimer phase to the z -FM phase is presented in Fig. 4a–c, which is characterized by the dimer order $\Delta_d^{54,56}$, magnetization M_η^{57} and entanglement entropy (EE). We define these two order parameters as

$$\Delta_d = \langle \mathbf{s}_i \cdot \mathbf{s}_{i+1} - \mathbf{s}_{i+1} \cdot \mathbf{s}_{i+2} \rangle, \quad M_\eta = \sum_i \langle s_i^\eta \rangle. \tag{20}$$

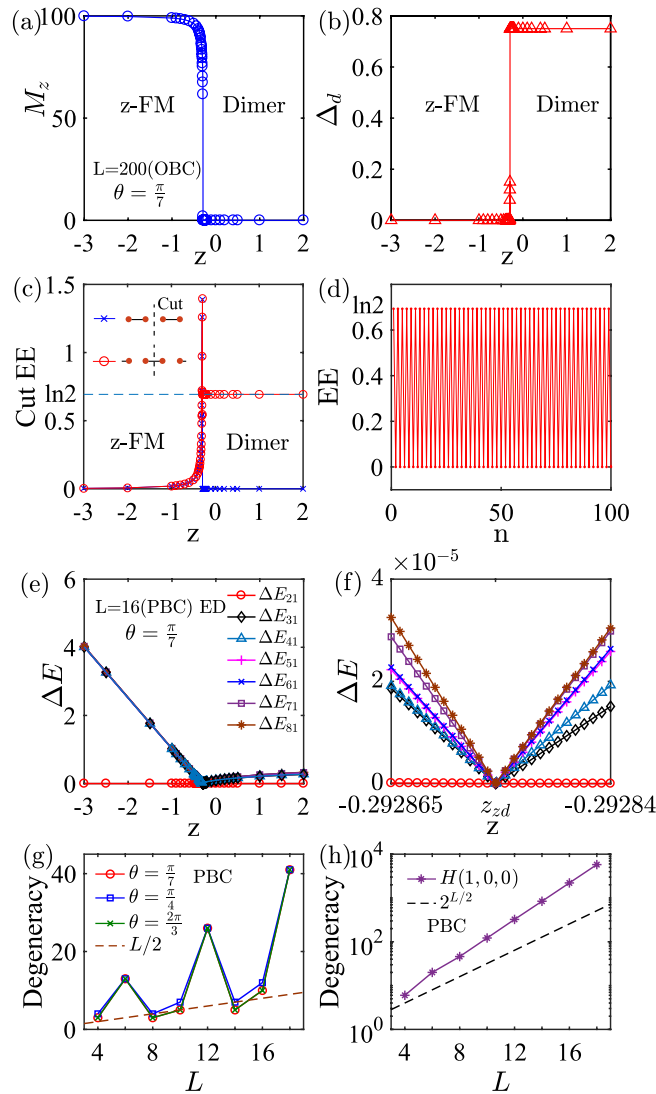


Figure 4. (a) Dimer and (b) magnetization orders at $\theta = \pi/7$ from density matrix renormalization group (DMRG) method with open boundary condition (OBC). The numerical determined boundary is $z_{ex} = -0.29283$, while the exact boundary from Eq. (13) is $z_c = -0.29285$. (c) The cut EE (see definition in the inset) as a function of z at $\theta = \pi/7$. At the phase boundary, the EE exhibits a sharp peak. (d) A typical result for oscillating of EE due to singlet dimer state. (e) Excitation gaps δE_{n1} from z -FM to exact dimer phase. (f) The enlarged excitation gaps near the critical point. Data are obtained for $L = 16$ from exact diagonalization (ED) with PBC. (g) The degeneracy of the GSs at the phase boundary as a function of L and θ , which scales as $\mathcal{O}(L/2)$. (h) The degeneracy of the GSs of $H(1, 0, 0)$ with scaling of $\mathcal{O}(2^{L/2})$.

Physically, the first order parameter reflects the translational symmetry breaking for dimerization; and the second one reflects the time reversal symmetry breaking for the FM phases. To further characterize the entanglement feature, or quantumness, in these phases, we can calculate the EE of a finite block A with size n , which is defined as^{58–60},

$$S_A(n) = -\text{Tr} \rho_A \ln \rho_A, \tag{21}$$

where ρ_A is the reduced density matrix by tracing out its complementary part. In the exact dimer phase, $\Delta_d = 3/4$, $M_z = 0$, and the central cut EE equals to 0 (at $n = L/2$) or $\ln 2$ (at $n = L/2 + 1$) due to formation of the singlet dimer state. In Fig. 4d, we show a typical result for oscillating of EE. In the z -FM phase, $M_z - L/2 \propto 1/z^2$ (from second-order perturbation theory), $\Delta_d = 0$; and with the decreases of z , the cut EE tends to be zero when z approaches the exact FM phase limit of $H(0, 0, -1)$ (see “Exact FM states”). The boundary determined by these order parameters is precisely the same as that from Eq. (13), with absolute difference less than 3×10^{-4} . The similar accuracy has been found for all dots at the boundaries in Fig. 2. In Fig. 4e,f, we show that at the phase boundary, the excitation gaps defined as $\delta E_{n1} = E_n - E_1$ for $n \geq 2$ collapse to zero, indicating of infinite-fold degeneracy when extending to infinite length. In Ref.⁴⁹, Gerhardt et al. have proven that the infinite-fold degeneracy of the GSs at point $x = y, z = -x/2$ by considering the n -magnon states

$$S^+(p)^n |FM\rangle_{\text{exact}}^z, \tag{22}$$

which can be obtained by n -fold application of the raising operator $S^+(p) = \sum_l e^{ip_l} s_l^+$. Here, $|FM\rangle_{\text{exact}}^z = |\downarrow\rangle^{\otimes L}$ is FM state (see also the more general definition in Eq. (31)). One can see that the n -magnon states are eigenstates of the Hamiltonian

$$H(x, x, -\frac{x}{2}) S^+(p)^n |FM\rangle_{\text{exact}}^z = E_g^{\text{FM}} S^+(p)^n |FM\rangle_{\text{exact}}^z, \tag{23}$$

for $p = 2\pi/3$ and $p = 4\pi/3$, where the FM state energy is given by

$$E_g^{\text{FM}} = -\frac{3xL}{16}. \tag{24}$$

This conclusion is achieved using

$$\begin{aligned} & \left[\left[H\left(x, x, -\frac{x}{2}\right), S^+(p) \right], S^+(p) \right] |FM\rangle_{\text{exact}}^z \\ & = -xe^{ip} [(1 + 2 \cos(p)) |2p, 1\rangle + e^{ip} \left(\frac{1}{2} + \cos(2p)\right) |2p, 2\rangle], \end{aligned} \tag{25}$$

where $|2p, j\rangle = \sum_l e^{2ip_l} |l, l+j\rangle$ are the two-magnon states with two spin excitations at sites l and $l+j$ (see Eq. 22). The right-band side disappears when $p = 2\pi/3$ and $p = 4\pi/3$. At this point, the eigenvalues E_g^{dimer} of the exact dimer states are degenerate with the energy E_g^{FM} of the FM states, which also implies that the n -magnon states are GSs of $H(x, x, -x/2)$. Thus the GSs energies are degenerate with respect to total spin $S_z = 0, 1, 2, \dots, L/2$ sectors⁴⁹. Therefore, in the thermodynamic limit, the degeneracy of the GSs is at least of the order of $\mathcal{O}(L/2)$. In Fig. 4g, we show the degeneracy of the GSs at the phase boundary with PBC. We find that the degeneracy increases with some kind of oscillation from the finite size effect with the increasing of L , which scales as $\mathcal{O}(L)$.

At the phase boundary, we also find three classical points $H(1, 0, 0)$, $H(0, 1, 0)$ and $H(0, 0, 1)$, with GSs degeneracy increases exponentially with the increasing of system size L . Here, $H(0, 0, 1)$ is relevant to the boundary defined in Eq. (13) in the limit of $x = -y$ and $z \rightarrow \infty$. Let us consider $H(x, 0, 0) = xH(1, 0, 0)$ for $x > 0$, and⁵⁵

$$H(1, 0, 0) = \frac{1}{2} \sum_i^L \sigma_i \sigma_{i+1} - \frac{L}{8}, \quad \sigma_i = \{-1, 0, 1\}, \tag{26}$$

where $\sigma_i = s_i^x + s_{i+1}^x$. This new operator takes three different values; however, the minimal value -1 from the product of the operators can not be reached due to the restriction $|\sigma_i - \sigma_{i+1}| = |s_i^x - s_{i+2}^x| = \{0, 1\}$. Thus $\sigma_i \sigma_{i+1} \geq 0$ and the GSs energy is $E_g = -L/8$. Let us consider a special case, that is, $\sigma_{2i} = 0$, and $\sigma_{2i+1} = \{1, 0\}$ or $\{-1, 0\}$. All these states have the same GSs energy $E_g = -L/8$. This means that the degeneracy of the GSs is at least of the order of $\mathcal{O}(2^{L/2})$, which is infinite-fold degenerate in infinite length (see verification in Fig. 4h). From this boundary, the system may undergo two different spontaneous symmetry breakings. When it breaks to the exact dimer phase, the system breaks the translational symmetry with $\Delta_d \neq 0$; while to the FM phases, it breaks the \mathbb{Z}_2 symmetry with $M_\eta \neq 0$ and $\Delta_d = 0$. Since we have three different \mathbb{Z}_2 operators for symmetry breaking, we have three different FM phases.

Ferromagnetic phases

We find three different FM phases polarize along the three orthogonal directions x, y and z . From the point of view of symmetry breaking, these FM phases correspond to the spontaneous \mathbb{Z}_2 symmetry breaking along the three axes. The transitions between them are phase transitions and the boundaries are gapless and critical. The three boundaries for the FM phases are $z = x$ for $\theta \in (\pi/2, 5\pi/4)$, $z = y$ for $\theta \in (5\pi/4, 2\pi)$, and $z > x = y = -1/\sqrt{2}$. Across these boundaries, the polarization of magnetizations will change direction. In the following, we use several complementary approaches to characterize these phase transitions.

Properties of FM phases. The phase boundaries of the three FM phases can be obtained by performing the dual transformation

$$\mathcal{R}_\eta = \prod_i \exp\left(i\frac{\pi}{2} s_i^\eta\right), \quad \eta = x, y, z. \tag{27}$$

For example, by performing \mathcal{R}_y , $H(x, y, z)$ is transferred to $H(z, y, x)$. This transformation means that the total Hamiltonian is invariant when $z = x$. Therefore, the boundaries are self-dual lines, which are gapless and critical. In order to verify these boundaries, we consider the EE in a finite chain with PBC as⁵⁸⁻⁶⁰,

$$S_A(n) = \frac{c}{3} \ln\left(\frac{L}{\pi} \sin \frac{\pi n}{L}\right) + s_0, \tag{28}$$

where c refers to central charge and s_0 is a non-universal constant. The results are presented in Fig. 5a,b. We find that the central charge $c = 1$ at the phase boundary, which is a typical feature of free fermions. In Fig. 5c, we show the central cut EE defined as $S(L/2)$ as a function of z at $\theta = 7\pi/6$ for different L and bond dimension m . At the phase boundary, we find that the EE exhibits a sharp peak, and its value increases with the increasing of lattice

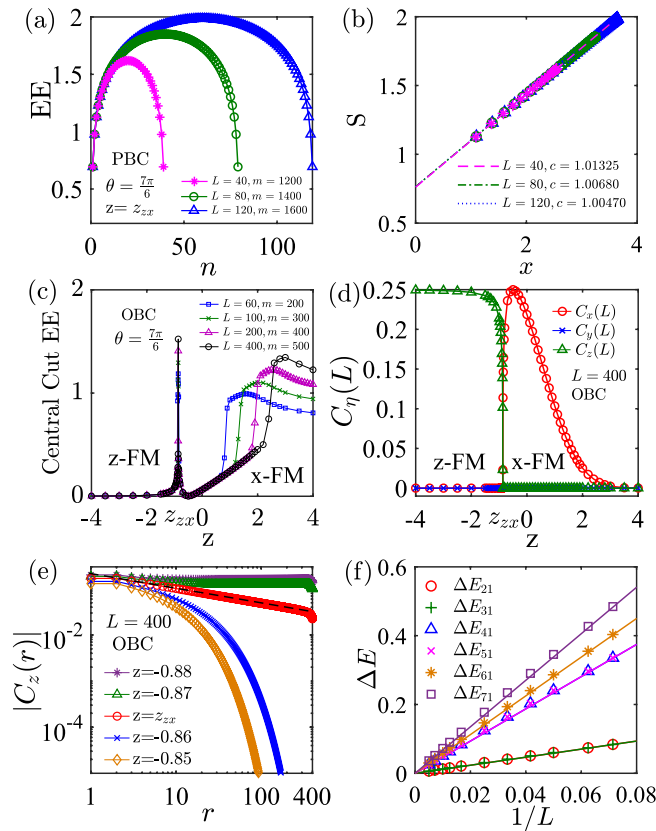


Figure 5. (a) and (b) show EE and central charge c at the boundary between z -FM and x -FM phase at $\theta = 7\pi/6$ with $z_{zx} = -0.86602$, by DMRG method with PBC. The dashed lines in (b) are fitted by Eq. (28) with $x = \ln(\frac{1}{\pi} \sin \frac{\pi n}{L})$, yielding $c = 1$. (c) Central cut EE as a function of z at $\theta = 7\pi/6$ for different L and bond dimension m . (d) Spin–spin correlation functions $C_\eta(L)$ ($\eta = x, y, z$) as a function of z at $\theta = 7\pi/6$ for $L = 400$. (e) Spin–spin correlation function $C_z(r)$ at $\theta = 7\pi/6$. At the phase boundary, $C_z(r) \propto |r|^{-0.32}$, by DMRG method with OBC. (f) Scaling of excitation gaps $\delta E_{n1} \propto 1/L$ for all n at the boundary ($\theta = 7\pi/6$ with $z_{zx} = -0.86602$) as a function of chain length, indicating of gapless and criticality.

site L , reflecting gapless and criticality. In the z -FM phase, with the decreasing of z , it will approach the exact FM phase limit $H(0, 0, -1)$, so the central cut EE tends to zero. However, in the x -FM phase, as z increases, the central cut EE first decreases (at the exact FM state point $z = \sin(7\pi/6)$, it equals to zero) and then increases (close to the infinite-fold degeneracy point $H(0, 0, 1)$); see details in “Order parameters and infinite-fold degeneracy”.

This phase transition may also be characterized by their long-range spin–spin correlation functions

$$C_\eta(r) = \langle s_1^\eta s_r^\eta \rangle, \quad \eta = x, y, z. \tag{29}$$

In Fig. 5d, we show the $C_\eta(L)$ as a function of z at $\theta = 7\pi/6$ for $L = 400$. As expected, in the z -FM phase, $C_{x,y}(L) = 0$ and $C_z(L) \neq 0$, while in the x -FM phase, $C_{y,z} = 0$ and $C_x(L) \neq 0$. In Fig. 5e, we study the correlation function $C_z(r)$ near the phase boundary. In the fully gapped z -FM phase with long-range order, this correlation function approaches a constant in the large separation limit. At the boundary, $C_z(r) \propto |r|^{-\gamma}$, which is a typical feature of critical phase. In the x -FM phase with spin polarization along x -direction, the correlation function $C_z(r)$ decays exponentially to zero; on the contrary, $\lim_{|r| \rightarrow \infty} C_x(r)$ approaches a constant.

We also study the excitation gaps, which is defined as the energy difference between the excited states and the ground state as

$$\Delta E_{n1} = E_n - E_1 = \Delta E_{n1}(\infty) + \frac{A_n}{L}, \quad n = 2, 3, \dots \tag{30}$$

At the phase boundaries, we find $\Delta E_{n1}(\infty) = 0$, which also means that the boundaries are gapless and critical (see Fig. 5f). These features are consistent with the finite central charge ($c = 1$) observed from central cut EE.

Exact FM states. There exist some special lines in the FM phases to support exact FM states as⁶¹

$$|\text{FM}\rangle_{\text{exact}}^\eta = |\eta\rangle^{\otimes L}, \tag{31}$$

where $|\eta\rangle$ is the eigenvector of s^η . As shown in Ref.⁴⁹, when $y = x > 0$ and $z < -x/2$, the ground state is an exact FM state spontaneously polarized along z -direction (thus breaks \mathbb{Z}_2 symmetry along z axis). In our model,

we also find another exact z -FM phase when $z < x = y = -1/\sqrt{2}$. This state can be mapped to the exact FM state along the other two directions by dual rotation $\mathcal{R}_{x,y}$, which induces permutation among the three directions. We find that the other two exact FM states at $z = y$ for $\theta \in (\pi - \arctan(2), 5\pi/4)$ and $z = x$ for $\theta \in (5\pi/4, 3\pi/2 + \arctan(2))$. These special cases are presented in Fig. 1 with dashed lines, in which the arrows mark the evolution of these dual mapping starting from $z \rightarrow -\infty$. One should be noticed that when $z \rightarrow -\infty$, it equals to $-H(0, 0, 1)$, which can be mapped to $-H(1, 0, 0)$ and $-H(0, 1, 0)$ by dual rotations. The GSs of these points should be two-fold degenerate with exact FM states in Eq. (31). This exact two-fold degeneracy can also be proven exactly by considering $-H(0, 0, 1)$ using the method in Eq. (26). In these exact FM states, the corresponding ground state energy can be written as

$$E_g^{\text{FM}} = -\frac{3L}{8} |\min\{x, y, z\}|. \quad (32)$$

Notice that the GSs of $-H(1, 1, 1)$ is infinite-fold degenerate, while in $H(1, 1, 1)$ it is exactly dimerized. This may provide an interesting example for the relation between the wave functions of the GSs and the highest energy states.

Experimental relevant and measurements

Let us finally discuss the relevance of this research to experiments in one dimensional magnets and their possible experimental signatures. The results in the previous sections are demonstrated at the exact MG point for the sake of exact solvability; however, these physics can be survived even when slightly away from this point, which can happen in real materials. These states are still characterized by the order parameter $\Delta_d \neq 0$ with a finite energy gap; however, it is no longer the exact dimer phase discussed before with wave function given in Eq. (7). These physics needs to be explored using numerical methods. In the spin-Peierls compounds, such as CuGeO_3 ³⁵, TiOCl ³⁷ and $(\text{TMTTF})_2\text{PF}_6$ ⁴¹, the strong anisotropy in lattice constants (for example, in CuGeO_3 the lattice constants are: $a = 8.4749 \text{ \AA}$, $b = 2.9431 \text{ \AA}$ and $c = 4.8023 \text{ \AA}$ ³⁶) is necessary to isolate a single Cu^{2+} chain (or other spin- $\frac{1}{2}$ ions) out from the three-dimensional bulk. For this reason, spatial anisotropy is inevitable and in order to describe real materials more accurately, anisotropy in the effective spin model is needed. In experiments, it was found that when the temperature is lower than the spin-Peierls transition temperature T_{sp} , the magnetic susceptibility in all directions will quickly drop to almost zero. Anisotropy in magnetic susceptibility will become significant in the FM phase when the Zeeman field exceeds a critical value or $T > T_{\text{sp}}$. In experiments, these observations are explained by an isotropic J_1 - J_2 model, which may support the dimer phase when $\alpha = J_2/J_1 > 0.2411$ ⁶². This isotropic model was also shown to be relevant to other anisotropic one dimensional magnets such as CuCrO_4 with $\alpha = 0.43$ ⁶³, BaV_3O_8 with $\alpha \approx 0.5$ ⁶⁴, $\text{Cu}_3(\text{MoO}_4)(\text{OH})_4$ with $\alpha = 0.45$ ³⁹, $\text{Cu}_6\text{Ge}_6\text{O}_{18} \cdot 6\text{H}_2\text{O}$ with $\alpha = 0.27$ ⁶⁵, $\text{Cu}_6\text{Ge}_6\text{O}_{18} \cdot \text{H}_2\text{O}$ with $\alpha = 0.29$ ⁶⁵ and $\text{Li}_{1.16}\text{Cu}_{1.84}\text{O}_{2.01}$ with $\alpha = 0.29$ ⁶⁶. In some of the experiments, anisotropy has been reported. For instance, in CuGeO_3 in Refs.⁴⁴⁻⁴⁶, the measured spin susceptibilities along the three crystal axes directions are different, differing by about 10–20%, and the parameters are determined to be $\alpha = 0.71$, $J_{xx} = 48.2 \text{ K}$, $J_{yy} = 47.2 \text{ K}$ and $J_{zz} = 49.7 \text{ K}$. In some materials, these parameters may even be negative valued. These results motivate us to think more seriously about the dimer phase in these compounds.

We model the experimental measurements by adding a magnetic field along η -direction,

$$H' = h \sum_i^L s_i^\eta, \quad \eta = x, y, z. \quad (33)$$

Since there is an energy gap $\delta E = E_3 - E_1$ in the exact dimer phase (note that $E_1 = E_2$ for \mathbb{Z}_2 symmetry), the external magnetic field will not immediately destroy the exact dimer phase. The magnetization M_η (see Eq. 20) for the exact dimer phase along different directions are presented in Fig. 6a. We find that the breakdown of the exact dimer phase takes place roughly at

$$h^c \simeq \delta E = E_3 - E_1. \quad (34)$$

When $h < h^c$, the magnetization $M_\eta = 0$ along different directions, thus $\chi_\alpha = \partial M_\alpha / \partial h = 0$. The anisotropy effect will be important in the region when $h > h^c$ or $T > T_{\text{sp}}$, which gives different susceptibilities for the magnetic field along different directions. This result is consistent with the experimental observations^{39, 68-71}. This anisotropy effect has been reported even in the first spin-Peierls compound CuGeO_3 ³⁴. In Fig. 6b, we show the magnetization M_η in the z -FM phase and find that even a small h can lead to a non-zero M_η . These features can be used to distinguish these fully gapped dimer and FM phases. In Fig. 6c, we plot the magnetization away from the MG point. The similar features can also be found in the dimer phase, and the phase transition can still take place at $h^c \simeq \delta E$. In experiments, the value of α depends strongly on the lattice constants, thus maybe tuned by temperature or external stress⁷². We plot the boundary for the dimer phase at $\theta = \frac{\pi}{7}$ and $z = -0.2$ in Fig. 6d, yielding $\alpha_c = 0.4362$ by extrapolation to infinite length using^{67, 73}

$$\alpha_c(L) - \alpha_c \propto L^{-2}. \quad (35)$$

We have also confirmed this boundary from the dimer order Δ_d and the long-range correlation function $C_\eta(r)$. This critical value is significantly larger than 0.2411 in the isotropic J_1 - J_2 model from the anisotropy effect. From the general theorem demonstrated in this work, we see that the dimer phase in the isotropic model will be survived even in the presence of anisotropy, thus it may find applications in the above materials.

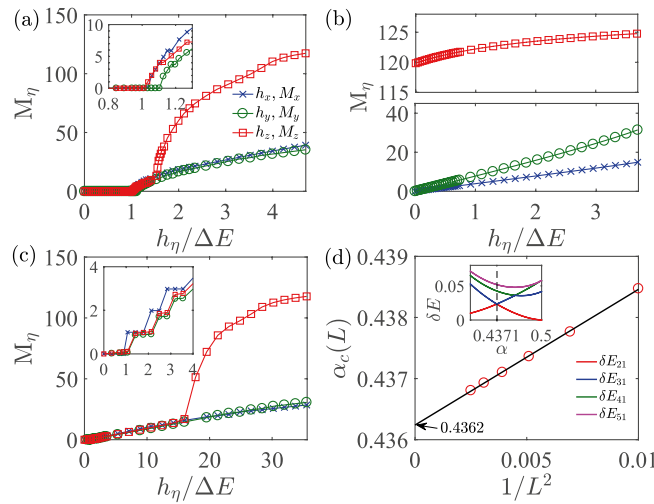


Figure 6. Magnetization M_η at $\theta = \frac{\pi}{7}$. **(a)** Exact dimer phase with $\alpha = \frac{1}{2}$, $z = -0.2$. The three critical Zeeman fields are $h_x^c = 0.044$, $h_y^c = 0.047$ and $h_z^c = 0.043$, and excitation gap $\delta E = 0.0425$. **(b)** z -FM phase with $\alpha = \frac{1}{2}$, $z = -0.4$, $\delta E = 0.054$. **(c)** Dimer phase with $\alpha = 0.45$, $z = -0.2$, $h_x^c = 0.005$, $h_y^c = 0.006$ and $h_z^c = 0.006$, $\delta E = 0.0056$. These results are obtained with $L = 256$ based on DMRG method. **(d)** Critical boundary for dimer phase at $\theta = \frac{\pi}{7}$ and $z = -0.2$. The critical point $\alpha_c = 0.4362$ is obtained by extrapolating to infinity length (see Eq. 35). Inset shows the boundary determined by level crossing between the first and second excited states⁶⁷.

Conclusion

This work is motivated by the generalization of the isotropic MG model to the anisotropic region, which may have applications in realistic one dimensional magnets. We demonstrate that the exact dimer phase can be found in a wide range of parameters in a generalized MG model (at point $\alpha = \frac{1}{2}$) with anisotropic XYZ interaction. Due to the presence of the exact dimer phase, the phase boundaries can be obtained analytically using simple models, which are verified with high accuracy using some numerical methods. We find that this model support one exact dimer phase and three FM phases, which polarize in different directions. The boundaries between the exact dimer phase and FM phases are infinite-fold degenerate, while between the FM phases are gapless, critical with central charge $c = 1$ for free fermions. These results may be relevant to a large number of one dimensional magnets. Possible signatures are presented to discriminate them in experiments. These results may advance our understanding of dimer phases in solid materials, and it may even have application in the searching of SPT phases^{74–77} from the general theorem proven in this manuscript.

Appendix

The major results in this work are established based on the following general theorem.

Theorem *When the Hamiltonians H_i have the same GS wave functions, then these GSs will also be the GSs of the Hamiltonian $H = \sum_i H_i$, in which these Hamiltonians H_i are not necessarily commutative to each other.*

We first prove this theorem using two Hamiltonians H_1 and H_2 , with corresponding GS wave functions as $|g_1\rangle$ and $|g_2\rangle$. Let us define $H = H_1 + H_2$, with GS as $|g\rangle$. Then

$$\begin{aligned} \langle g|H|g\rangle &= \langle g|H_1 + H_2|g\rangle = \langle g|H_1|g\rangle + \langle g|H_2|g\rangle \\ &\geq \langle g_1|H_1|g_1\rangle + \langle g_2|H_2|g_2\rangle. \end{aligned} \tag{36}$$

In particular when H_1 and H_2 have the same GSs that $|g'\rangle = |g_1\rangle = |g_2\rangle$, then Eq. (36) can be further written as

$$\begin{aligned} \langle g|H|g\rangle &\geq \langle g'|H_1|g'\rangle + \langle g'|H_2|g'\rangle \\ &= \langle g'|H_1 + H_2|g'\rangle = \langle g'|H|g'\rangle. \end{aligned} \tag{37}$$

This means that $|g'\rangle$ is the ground state of H . This conclusion can be generalized to an arbitrary number of Hamiltonians H_i with $i = 1, \dots, n$ for $n > 2$, in which $H = \sum_i H_i$ will have the same GSs as H_i . In the main text of Eq. (17), the GSs of $H(x', x', z')$ and $H(x'', y'', 0)$ are exact dimerized with wave functions defined in Eq. (7), so the GSs of H_x should also be the same dimerized states, following this general theorem.

It should be emphasized that in the above theorem, the different Hamiltonians H_i are not necessarily to be commutative to each other. In the main text, we have used two different Hamiltonians $H_1 = H(x', x', z')$ and $H_2 = H(x'', y'', 0)$, which have the same GSs; however, $[H_1, H_2] \neq 0$. For this reason, this theorem should be different from the concept of the complete set of commuting observables (CSCO) used in textbooks, which state that when two operators H_1 and H_2 are commutate, then they will have the common eigenvectors; however, these

two Hamiltonians may have different GSs. For instance, if we define a folded Hamiltonian as $H_2 = (H_1 - \epsilon)^2$. Apparently, $[H_2, H_1] = 0$. However, the GS of H_2 may correspond to the excited state of H_1 with energy closes to ϵ . Another example, which is much simpler, is $H_2 = -H_1$, in which the GS of H_1 is the highest energy state of H_2 ; and vice versa.

This theorem can be used to explain a part of the exact dimer phase in the phase diagram (see the light red regions in Fig. 1), but not all. We can define $x = \cos(\theta)$ and $y = \sin(\theta)$ (see Fig. 2), then we have the following three cases. These cases have been verified by numerical simulation. We find that including much more decouplings will not change these conclusions; in other words, the deep red regions in Fig. 2 can not be explained by this decoupling.

- (1) For $\theta \in [0, \pi/2]$; if $z > 0$, we have decoupling as

$$H(x, y, z) = H\left(\frac{x}{2}, \frac{y}{2}, 0\right) + H\left(\frac{x}{2}, 0, \frac{z}{2}\right) + H\left(0, \frac{y}{2}, \frac{z}{2}\right). \quad (38)$$

However, if $z \leq 0$, we have

$$H(x, y, z) = H(-2z, -2z, z) + H(x + 2z, y + 2z, 0), \quad (39)$$

where $H(-2z, -2z, z)$ locates at the phase boundary of XXZ model. Therefore, if the GSs of $H(x, y, z)$ are exact dimer states, $H(x + 2z, y + 2z, 0)$ should satisfy $x + 2z > 0$ and $y + 2z > 0$, which yields

$$z > -\frac{1}{2} \min(\cos(\theta), \sin(\theta)). \quad (40)$$

- (2) For $\theta \in (\pi/2, \pi]$, we can make a unitary transformation \mathcal{R}_y , which transfers $H(x, y, z)$ to $H(z, y, x)$, then

$$H(z, y, x) = H(-2x, -2x, x) + H(z + 2x, y + 2x, 0). \quad (41)$$

In order to ensure that the GSs of $H(x, y, z)$ are exact dimer states, the condition $z + 2x > 0$ and $y + 2x > 0$ need to be satisfied, yielding

$$\theta \in (\pi/2, \pi - \arctan(2)), \quad z > -2 \cos(\theta). \quad (42)$$

- (3) For $\theta \in [3\pi/2, 2\pi]$, the exact dimer states can be obtained in a similar method by a unitary transformation \mathcal{R}_x , the exact dimer phase requires

$$\theta \in (3\pi/2 + \arctan(2), 2\pi), \quad z > -2 \sin(\theta). \quad (43)$$

The above three conditions have been used at the end of “Phase boundary”, indicating that the deep red regions in the phase diagram can not be understood based on this approach.

This general theorem may have much broader applications because the validity of this theorem can be applied to diverse physical models, including the single-particle models as well as the many-body models. It only requires that the Hamiltonians H_i have the same GSs, so it may also have potential application in the construction of SPT phases.

Received: 15 October 2020; Accepted: 25 February 2021

Published online: 19 March 2021

References

- Auerbach, A. *Interacting Electrons and Quantum Magnetism* (Springer, 2012).
- Baxter, R. J. *Exactly Solved Models in Statistical Mechanics* (Elsevier, 2016).
- Amico, L., Fazio, R., Osterloh, A. & Vedral, V. Entanglement in many-body systems. *Rev. Mod. Phys.* **80**, 517 (2008).
- Pfeuty, P. The one-dimensional Ising model with a transverse field. *Ann. Phys.* **57**, 79–90 (1970).
- Cheng, J.-M., Zhou, X.-F., Zhou, Z.-W., Guo, G.-C. & Gong, M. Symmetry-enriched Bose-Einstein condensates in a spin-orbit-coupled bilayer system. *Phys. Rev. A* **97**, 013625 (2018).
- Cao, J.-P., Cui, S., Yang, W.-L., Shi, K.-J. & Wang, Y.-P. Spin-1/2 XYZ model revisit: General solutions via off-diagonal Bethe ansatz. *Nucl. Phys. B* **886**, 185–201 (2014).
- Ercolessi, E., Evangelisti, S., Franchini, F. & Ravanini, F. Essential singularity in the renyi entanglement entropy of the one-dimensional xyz spin-1/2 chain. *Phys. Rev. B* **83**, 012402 (2011).
- Ercolessi, E., Evangelisti, S., Franchini, F. & Ravanini, F. \Modular invariance in the gapped xyz spin-12 chain. *Phys. Rev. B* **88**, 104418 (2013).
- Kitaev, A. Y. Fault-tolerant quantum computation by anyons. *Ann. Phys.* **303**, 2–30 (2003).
- Kitaev, A. \Anyons in an exactly solved model and beyond. *Ann. Phys.* **321**, 2–111 (2006).
- Batista, C. & Ortiz, G. Generalized Jordan–Wigner transformations. *Phys. Rev. Lett.* **86**, 1082 (2001).
- Tzeng, Y.-C., Dai, L., Chung, M.-C., Amico, L. & Kwek, L.-C. Entanglement convertibility by sweeping through the quantum phases of the alternating bonds XXZ chain. *Sci. Rep.* **6**, 26453 (2016).
- Karbach, P. & Stolze, J. Spin chains as perfect quantum state mirrors. *Phys. Rev. A* **72**, 030301 (2005).
- Yao, N. Y. *et al.* Robust quantum state transfer in random unpolarized spin chains. *Phys. Rev. Lett.* **106**, 040505 (2011).
- Mukherjee, V., Divakaran, U., Dutta, A. & Sen, D. Quenching dynamics of a quantum XY spin-1/2 chain in a transverse field. *Phys. Rev. B* **76**, 174303 (2007).
- Lieb, E. H. & Wu, F. Y. Absence of mott transition in an exact solution of the short-range, one-band model in one dimension. *Phys. Rev. Lett.* **20**, 1445 (1968).
- Mourigal, M. *et al.* Fractional spinon excitations in the quantum heisenberg antiferromagnetic chain. *Nat. Phys.* **9**, 435 (2013).
- Wang, Z. *et al.* Experimental observation of bethe strings. *Nature* **554**, 219 (2018).

19. Wang, Z. *et al.* Spinon confinement in the one-dimensional Ising-like antiferromagnet SrCo₂V₂O₈. *Phys. Rev. B* **91**, 140404 (2015).
20. Osterloh, A., Amico, L., Falci, G. & Fazio, R. Scaling of entanglement close to a quantum phase transition. *Nature* **416**, 608 (2002).
21. Vidal, G., Latorre, J. I., Rico, E. & Kitaev, A. Entanglement in quantum critical phenomena. *Phys. Rev. Lett.* **90**, 227902 (2003).
22. Bonnes, L., Essler, F. H. L. & Läuchli, A. M. “Light-cone” dynamics after quantum quenches in spin chains. *Phys. Rev. Lett.* **113**, 187203 (2014).
23. Bertini, B., Collura, M., De Nardis, J. & Fagotti, M. Transport in out-of-equilibrium XXZ chains: Exact profiles of charges and currents. *Phys. Rev. Lett.* **117**, 207201 (2016).
24. Majumdar, C. K. & Ghosh, D. K. On Next-Nearest-Neighbor interaction in linear chain. I. *J. Math. Phys.* **10**, 1388–1398 (1969).
25. Majumdar, C. K. & Ghosh, D. K. On Next-Nearest-Neighbor interaction in linear chain. II. *J. Math. Phys.* **10**, 1399–1402 (1969).
26. Chhajlany, R. W., Tomczak, P., Wójcik, A. & Richter, J. Entanglement in the Majumdar–Ghosh model. *Phys. Rev. A* **75**, 032340 (2007).
27. Liu, G.-H., Wang, C.-H. & Deng, X.-Y. Quantum entanglement and quantum phase transitions in frustrated Majumdar–Ghosh model. *Physica B Condens. Matter* **406**, 100–103 (2011).
28. Lavaré, A. & Roux, G. Localization of spinons in random Majumdar–Ghosh chains. *Phys. Rev. Lett.* **110**, 087204 (2013).
29. Ramkarthik, M., Chandra, V. R. & Lakshminarayan, A. Entanglement signatures for the dimerization transition in the Majumdar–Ghosh model. *Phys. Rev. A* **87**, 012302 (2013).
30. Affleck, I., Kennedy, T., Lieb, E. H., & Tasaki, H. Valence bond ground states in isotropic quantum antiferromagnets. in *Condensed Matter Physics and Exactly Soluble Models: Selecta of Elliott H. Lieb*, (eds Nachtergaele, B., Solovej, J. P. & Yngvason, J.) 253–304 (Springer Berlin Heidelberg, Berlin, Heidelberg, 2004).
31. Santos, R. A., Korepin, V. & Bose, S. Negativity for two blocks in the one-dimensional spin-1 Affeck–Kennedy–Lieb–Tasaki model. *Phys. Rev. A* **84**, 062307 (2011).
32. Morimoto, T., Ueda, H., Momoi, T. & Furusaki, A. Z₃ symmetry-protected topological phases in the SU(3) AKLT model. *Phys. Rev. B* **90**, 235111 (2014).
33. Wei, T.-C., Affeck, I. & Raussendorf, R. Affeck–Kennedy–Lieb–Tasaki state on a honeycomb lattice is a universal quantum computational resource. *Phys. Rev. Lett.* **106**, 070501 (2011).
34. Hase, M., Terasaki, I. & Uchinokura, K. Observation of the spin-Peierls transition in linear Cu²⁺ (spin-1/2) chains in an inorganic compound CuGeO₃. *Phys. Rev. Lett.* **70**, 3651–3654 (1993).
35. O’Neal, K. R. *et al.* Vibronic coupling and band gap trends in CuGeO₃ nanorods. *Phys. Rev. B* **96**, 075437 (2017).
36. Meibohm, M. & Otto, H. H. Comparison of the vibrational spectra of copper polysilicate, CuSiO₃, with those of the prototypic copper polygermanate, CuGeO₃. *AJAC* **9**, 311 (2018).
37. Rotundu, C. R. *et al.* Enhancement and destruction of spin-Peierls physics in a one-dimensional quantum magnet under pressure. *Phys. Rev. B* **97**, 054415 (2018).
38. Zhang, J. *et al.* Transformation between spin-Peierls and incommensurate modulating phases of Sc-doped TiOCl. *Phys. Rev. B* **90**, 014415 (2014).
39. Lebernegg, S. *et al.* Frustrated spin chain physics near the Majumdar–Ghosh point in szenicsite Cu₃(MoO₄)(OH)₄. *Phys. Rev. B* **95**, 035145 (2017).
40. Inagaki, Y. *et al.* Phase diagram and soliton picture of a spin-Peierls compound DF5PNN. *J. Phys. Soc. Jpn.* **86**, 113706 (2017).
41. Pouget, J. *et al.* Inelastic neutron scattering investigation of magnetostructural excitations in the spin-Peierls organic system (TMTTF)₂PF₆. *Phys. Rev. B* **96**, 035127 (2017).
42. Jeannin, O. *et al.* Decoupling anion-ordering and spin-Peierls transitions in a strongly one-dimensional organic conductor with a chessboard structure, (o-Me₂TTF)₂NO₃. *IUCr* **5**, 361–372 (2018).
43. Poirier, M., de Lafontaine, M., Bourbonnais, C. & Pouget, J.-P. Charge, spin, and lattice effects in the spin-Peierls ground state of MEM(TCNQ)₂. *Phys. Rev. B* **88**, 245134 (2013).
44. Miljak, M., Herak, M., Revcolevschi, A. & Dhalenne, G. Anisotropic spin-Peierls state in the inorganic compound CuGeO₃. *Europhys. Lett.* **70**, 369 (2005).
45. Wang, F., Xing, Y., Su, Z. & Song, S. Single-crystalline CuGeO₃ nanorods: Synthesis, characterization and properties. *Mater. Res. Bull.* **48**, 2654–2660 (2013).
46. Kremer, R. K. Anisotropic decrease of the spin-Peierls transition temperature of CuGeO₃ with a magnetic field. *Solid State Commun.* **96**, 427–430 (1995).
47. Kanter, I. Exact ground state of a class of quantum spin systems. *Phys. Rev. B* **39**, 7270–7272 (1989).
48. Nomura, K. & Okamoto, K. Phase diagram of S = 1/2 antiferromagnetic XXZ chain with Next-Nearest-Neighbor interactions. *J. Phys. Soc. Jpn.* **62**, 1123–1126 (1993).
49. Gerhardt, C., Mütter, K.-H. & Kröger, H. Metamagnetism in the XXZ model with next-to-nearest-neighbor coupling. *Phys. Rev. B* **57**, 11504–11509 (1998).
50. Kumar, B. Quantum spin models with exact dimer ground states. *Phys. Rev. B* **66**, 024406 (2002).
51. Hindmarsh, M., Rummukainen, K. & Weir, D. J. New solutions for non-Abelian cosmic strings. *Phys. Rev. Lett.* **117**, 251601 (2016).
52. Politis, E., Tsagkarakis, C., Diakonou, F., Maitas, X. & Tsapalis, A. A non-Abelian quasi-particle model for gluon plasma. *Phys. Lett. B* **763**, 139–144 (2016).
53. Gils, C. *et al.* Collective states of interacting anyons, edge states, and the nucleation of topological liquids. *Phys. Rev. Lett.* **103**, 070401 (2009).
54. Furukawa, S., Sato, M., Onoda, S. & Furusaki, A. Ground-state phase diagram of a spin-1/2 frustrated ferromagnetic XXZ chain: Haldane dimer phase and gapped/gapless chiral phases. *Phys. Rev. B* **86**, 094417 (2012).
55. Zhang, S.-Y. *et al.* Topological phase, supercritical point, and emergent phenomena in an extended parafermion chain. *Phys. Rev. B* **100**, 125101 (2019).
56. Michaud, F., Vernay, F., Manmana, S. R. & Mila, F. Antiferromagnetic spin-S chains with exactly dimerized ground states. *Phys. Rev. Lett.* **108**, 127202 (2012).
57. De Chiara, G., Lepori, L., Lewenstein, M. & Sanpera, A. Entanglement spectrum, critical exponents, and order parameters in quantum spin chains. *Phys. Rev. Lett.* **109**, 237208 (2012).
58. Holzhey, C., Larsen, F. & Wilczek, F. Geometric and renormalized entropy in conformal field theory. *Nucl. Phys. B* **424**, 443–467 (1994).
59. Jünemann, J. *et al.* Exploring interacting topological insulators with ultracold atoms: The synthetic Creutz–Hubbard model. *Phys. Rev. X* **7**, 031057 (2017).
60. Calabrese, P. & Cardy, J. Entanglement entropy and conformal field theory. *J. Phys. A Math. Theor.* **42**, 504005 (2009).
61. By assuming the exact state to be $(\cos(\theta/2)e^{i\phi/2}, \sin(\theta/2)e^{i\phi/2})^{T\otimes L}$ and minimize the corresponding ground state energy with respect to parameters θ and ϕ , we find that for the exact FM phase, the spin can only polarize along x , y and z directions.
62. Bursill, R. *et al.* Numerical and approximate analytical results for the frustrated spin-1/2 quantum spin chain. *J. Phys. Condens. Matter* **7**, 8605 (1995).
63. Law, J. *et al.* Quasi-one-dimensional antiferromagnetism and multiferroicity in CuCrO₄. *Phys. Rev. B* **84**, 014426 (2011).
64. Chakrabarty, T. *et al.* BaV₃O₈: A possible Majumdar–Ghosh system with $s = 1/2$. *Phys. Rev. B* **88**, 014433 (2013).
65. Hase, M., Ozawa, K. & Shinya, N. Magnetic properties of Cu_xGe_{6-x}O_{18-2x}·H₂O ($x = 0-6$): A compound of $s = 1/2$ Heisenberg competing antiferromagnetic chains coupled by interchain interaction. *Phys. Rev. B* **68**, 214421 (2003).

66. Masuda, T., Zheludev, A., Bush, A., Markina, M. & Vasiliev, A. Competition between helimagnetism and commensurate quantum spin correlations in LiCu_2O_2 . *Phys. Rev. Lett.* **92**, 177201 (2004).
67. Somma, R. & Aligia, A. Phase diagram of the XXZ chain with next-nearest-neighbor interactions. *Phys. Rev. B* **64**, 024410 (2001).
68. Ryu, G. & Son, K. Surface defect free growth of a spin dimer TlCuCl_3 compound crystals and investigations on its optical and magnetic properties. *J. Solid State Chem.* **237**, 358–363 (2016).
69. Zayed, M. E. *et al.* 4-spin plaquette singlet state in the Shastry–Sutherland compound $\text{SrCu}_2(\text{BO}_3)_2$. *Nat. Phys.* **13**, 962 (2017).
70. Yamaguchi, H. *et al.* Various regimes of quantum behavior in an $s = 1/2$ Heisenberg antiferromagnetic chain with fourfold periodicity. *Phys. Rev. B* **88**, 174410 (2013).
71. Sahling, S. *et al.* Experimental realization of long-distance entanglement between spins in antiferromagnetic quantum spin chains. *Nat. Phys.* **11**, 255 (2015).
72. Martin, N., Regnault, L.-P., Klimko, S., Lorenzo, J. & Gähler, R. Larmor diffraction measurement of the temperature dependence of lattice constants in CuGeO_3 . *Physica B Condens. Matter.* **406**, 2333–2336 (2011).
73. Riera, J. & Dobry, A. Magnetic susceptibility in the spin-Peierls system CuGeO_3 . *Phys. Rev. B* **51**, 16098–16102 (1995).
74. Chen, X., Gu, Z.-C. & Wen, X.-G. Classification of gapped symmetric phases in one-dimensional spin systems. *Phys. Rev. B* **83**, 035107 (2011).
75. Chen, X., Zheng-Cheng, Gu., Liu, Z.-X. & Wen, X.-G. Symmetry protected topological orders and the group cohomology of their symmetry group. *Phys. Rev. B* **87**, 155114 (2013).
76. Chen, X., Gu, Z.-C., Liu, Z.-X. & Wen, X.-G. Symmetry-protected topological orders in interacting bosonic systems. *Science* **338**, 1604–1606 (2012).
77. Chen, X., Gu, Z.-C. & Wen, X.-G. Complete classification of one-dimensional gapped quantum phases in interacting spin systems. *Phys. Rev. B* **84**, 235128 (2011).

Acknowledgements

This work is supported by the National Key Research and Development Program in China (Grant Nos. 2017YFA0304504 and 2017YFA0304103) and the National Natural Science Foundation of China (NSFC) with No. 11774328.

Author contributions

H.X. and S.Z. performed the theoretical calculation. G.G. and M.G. conceived the idea and supervised the project. All authors contributed to write the manuscript.

Competing interests

The authors declare no competing interests.

Additional information

Correspondence and requests for materials should be addressed to M.G.

Reprints and permissions information is available at www.nature.com/reprints.

Publisher's note Springer Nature remains neutral with regard to jurisdictional claims in published maps and institutional affiliations.



Open Access This article is licensed under a Creative Commons Attribution 4.0 International License, which permits use, sharing, adaptation, distribution and reproduction in any medium or format, as long as you give appropriate credit to the original author(s) and the source, provide a link to the Creative Commons licence, and indicate if changes were made. The images or other third party material in this article are included in the article's Creative Commons licence, unless indicated otherwise in a credit line to the material. If material is not included in the article's Creative Commons licence and your intended use is not permitted by statutory regulation or exceeds the permitted use, you will need to obtain permission directly from the copyright holder. To view a copy of this licence, visit <http://creativecommons.org/licenses/by/4.0/>.

© The Author(s) 2021